

Computer-aided discrimination of slow and fast tracer paths

H.-H. Bartels-Lehnhoff, W. J. Hiller and T. A. Kowalewski

Max-Planck-Institut für Strömungsforschung, Bunsenstr. 10, D-3400 Göttingen, Germany

Abstract. An optical method for the discrimination between slow and fast tracer particles convected within a flow is proposed. It is based on the dependence of the brightness of a trace on the velocity of the corresponding tracer. The images of the traces are captured by a CCD-camera and processed on-line. A practical application of this technique to the visualization of the low velocity streamlines in a rotating duct is presented. The possibilities to develop this technique into a quantitative tool for velocity measurements is discussed.

1 Introduction

Visualization of streamline patterns by imaging tracer particles suspended in the flow medium is one of the classical but still widely used observation technique in fluid mechanics. The methods are documented in many textbooks, e.g. Adrian (1988), Merzkirch (1974), Wuest (1969), and the impressive photos of the transition to turbulence by Reynolds (1833) are well known to the fluid dynamic community. Visualization of the streamlines, however, often becomes complicated in the presence of large spatial velocity variations within the probe volume. Under such conditions, the field of view is either crowded with a large number of traces due to rapid moving particles or the low speed traces become quite rare. Unfortunately, such situations will occur for flow structures like stagnation or recirculation regions in three-dimensional flow fields, or in the neighbourhood of other singular points where the low speed particles are of special interest. These difficulties could be reduced if one would provide a fast and operative method for separating the tracks of the rapid particles from the slow ones. Since a “slow” track will be brighter than a “rapid” one – we assume that the particles are illuminated by continuous light – it seems worthwhile to attempt a classification of the traces by their brightness. It is obvious that for large observation times or very high tracer particle densities the scattered light collected on the recording medium will finally become homogeneously distributed. From such images, of course, detailed information on the traces can no longer be extracted. Part of the work will

therefore be related to providing rules of thumb for practical results.

As an appropriate recording medium for the capture of the particle tracks CCD-cameras seem to be suited best. Their advantage over conventional photographic recording film is mainly due to the linear response of a CCD to the incoming light. In combination with a frame grabber one gets the immediate availability of the images for further computer aided signal conditioning and analysis.

2 Description of the method

2.1 Intensity of a trace

Let Φ_p be the luminant flux scattered from a single tracer that is focused by the imaging lens of a CCD-camera on one pixel of the sensor matrix. For simplicity, we assume that the probe volume is homogeneously illuminated and that the luminant flux Φ_p across the entire image of a tracer is constant. Furthermore, the size of a pixel is small compared to the size of a particle image. For a particle at rest and for displacements – within the plane of observation – smaller than the dimension of the image of the particle there will be locations on its trace that are illuminated during the entire integration time t_E of the camera. There, the energy E_p collected on a pixel during time t_E will be $E_p = \Phi_p \cdot t_E$. For displacements larger than the tracer image, the energy accumulated by a pixel will decrease by a factor of $L_p/(|v_p| \cdot t_E)$. This factor is the ratio between the length L_p of the tracer image measured in the direction of its motion – imagine for instance a needle shaped image of length L_p moving along its axis- and the displacement $|v_p| \cdot t_E$ of the particle image. v_p is the velocity of the particle image observed on the sensor of the camera at the location of the corresponding pixel. For E_p that is directly proportional to the electric output signal of the CCD-camera the following expressions result:

$$E_p = \Phi_p \cdot t_E \quad \text{for } L_p/(|v_p| \cdot t_E) \geq 1 \quad (1)$$

$$E_p = \Phi_p \cdot L_p/|v_p| \quad \text{for } L_p/(|v_p| \cdot t_E) \leq 1 \quad (2)$$

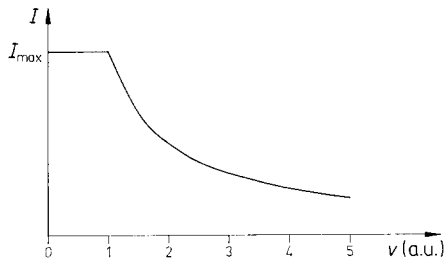


Fig. 1. Calculated maximum brightness I_{\max} of a trace versus its velocity v in arbitrary units. Tracers are observed against a black background

This hyperbolic relation (Fig. 1) between the energy E_p and the modulus of the velocity v_p is optimally suited for the identification of velocities at the lower end of the operating range. The minimum detectable velocity $v_{p\min}$ is given by the condition in Eq. (2). For a tracer particle of diameter $D = 100 \mu\text{m}$ and an exposure time of $t_E = 40 \text{ ms}$ (integration time of an interline CCD-camera) the corresponding particle velocity $v_{p\min}$ measured from the intensity of the center of the trace will become:

$$|v_{p\min}| = 2.5 \text{ mm/s} \quad (3)$$

A further reduction of this lower velocity limit could be reached in principle either by choosing smaller particles or larger integration times. The first of these possibilities is already realized if spherical particles are used, as the effective length L_p of its image decreases continuously of the lateral regions of the trace. However, one has to be careful with the selection of the physical parameters as will be discussed later. The highest velocity that may be evaluated by this method, depends, for a given particle size, on the dynamic range of the output signal of the camera.

A similar dependence for the brightness holds if the particles are viewed against a bright background. A particle at rest becomes visible as a dark dot. The higher the velocities the brighter the trace will be (Fig. 2). For both methods the intensity of the light source has to be adjusted such that the dynamic range of the CCD is not exceeded. In the neighbourhood of singular points, where the flow velocity is close to zero, the length of the traces captured during 40 ms often may become so short that flow structures cannot be identified. Then a continuous series of images has to be taken.

2.2 Capture of the images

The camera that is used for the present experiments is of the interline type (Sony XC-77CE). Its gain is kept fixed as light intensities are to be measured. To make best use of its dynamic range the intensity of the illuminating light source has to be carefully adjusted.

The optical sensitive picture elements (pixels) are arranged in a frame of 581 horizontal lines and 756 vertical columns. The size of a pixel is $11 \times 11 \mu\text{m}$. The frame is subdivided into two fields, one containing the odd numbered

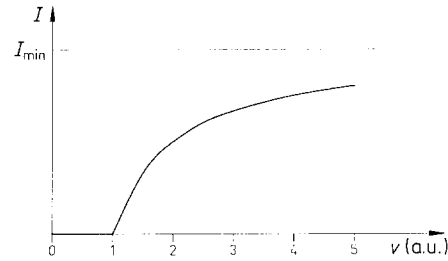


Fig. 2. Calculated minimum brightness I_{\min} of a trace versus its velocity v . Tracers are observed against a bright background

lines and the other the even ones. The camera is operated in the interlaced frame integration mode that gives the highest spatial resolution. On each of the two fields the oncoming light is collected for 40 ms. The integration periods of the fields overlap for 20 ms. Therefore, the information contained in one full image (frame) covers a period of 60 ms. For the first and last 20 ms of one frame only the odd or the even fields are exposed, respectively. For the centre 20 ms the exposure period of the two fields coincides. In this part of the frame the information is stored in the even and odd lines. Depending on which of the two fields of a frame a common trace appears first one can detect the direction of motion in the plane of observation.

The objective lens used in the present experiments has a focal length of 75 mm. The images are taken at a scale of 1:0.22 (i.e. 1 cm in physical space of the probe volume corresponds to 0.22 cm on the sensor of the CCD-camera) if not otherwise stated. If an image either from the camera or from the storage is displayed on a video-print it becomes automatically enlarged by a factor of 11.2. In order to show the pixel structure of an object (e.g. Fig. 8b), a higher enlargement is necessary. This can be achieved by the image processing software. If we have made use of this possibility we indicate it by the attribute "expanded view". The expanded view like the enlargement by a videoprint does not result into finer resolution of the object.

Depending on the aperture of the lens the depth of field of view changes and the resolution is limited by diffraction. For a value of the light stop of $f: 3.8$, $f: 8$, and $f: 16$ the measured depth of the focus is approximately 5 mm, 10 mm, and 15 mm and the theoretical resolution on the plane of the CCD-sensor calculated for optical illumination will be in the range of $3 \mu\text{m}$, $6 \mu\text{m}$, and $13 \mu\text{m}$, respectively. The effective wavelength of the illumination light source is assumed to be 600 nm.

For the case that a tracer is out of focus, the intensity of its images will become smaller than for a correctly focused one. This implies that the depth of focus with respect to the field of view must be adequately chosen. On the other hand, if the probe volume is embedded into an extensive flow field, a suitable adjustment of the focus may help to reduce interference with traces originating from outside the probe volume.

Similar problems result from particles of different size. For the case that the images of the tracers become comparable to its diffraction disk, their intensity will decrease. Also the intensity of a particle image that is in the range of the pixel dimensions will heavily fluctuate according to the number of pixels it momentarily hits but not completely covers.

2.3 Classification of the traces

The images captured by the CCD-camera are acquired on-line by the 8-bit A/D-converter of a VFG-100 image processing board. An accomodation of the video signal with respect to gain and offset is possible. The digitized images may be stored directly in the image memory or they can also first be classified on-line and afterwards stored. The available memory of $1\text{ K} \times 1\text{ K} \times 12\text{ Bit}$ allows to store either two frames of 768×512 pixels with a depth of 8 Bits or 24 binary images with the same spatial resolution.

Processing of the images is performed with look-up tables which are today a common feature of frame grabbers. A detailed description of the use and application of image processing by means of frame grabbers can be found e.g. in Bartels-Lehnhoff (1991), Brodkey (1986), Jähne (1989). The classification applied here consists in comparing the values of the intensity of the traces with an upper and a lower threshold. The sections of the traces with intensities between these limits are preserved, and the constituent pixels are encoded with respect to their intensity in colour or in such a way that they become clearly visible on a monitor or other display facilities. The intensity of the remaining pixels is set to zero. The resulting binary images are stored. Depending on the thresholds selected, flow velocity, particle number density, and time of observation the traces may more or less frequently cross each other. If in these points the intensity is higher than the upper threshold the intersection of the traces will become visible as dark points. The crossings may also rise up as isolated bright points if their level is inside the filter bandwidth and those of the corresponding traces below the lower threshold. Finally, they may also remain unaffected if the intensities of the intersection and of one of the traces are within the bandwidth of the filter. In most cases visualization is not disturbed if the number of such spots is not too high. A corresponding relation holds for the observation in the bright field mode.

In general, a normal CCD-camera is expected to cover a dynamic range of 8 bits or 256 grey levels. From practical experience, however, it is more realistic to assume a resolution of 6 bits or 64 grey levels. For a particle of $100\ \mu\text{m}$ this implies a velocity range from 0 to 160 mm/s divided into 64 ranges. In the first range one will find the particles with velocities between 0 and 2.5 mm/s (Eq. 2) and in the last one all particles with velocities higher than 160 mm/s, as long as their image intensity is not buried in the noise.

For the case that the traces captured during 40 ms are too short so that a continuous series of images is needed, one

preferably performs first classification of the traces and then superposition of their images. Otherwise the dynamics of the resulting image will be reduced as has been explained above.

2.4 Selection of the tracer particles

Usually, tracer particles will not be uniform in size and may also deviate considerably from a spherical shape. In these cases the brightness of the traces depends on the actual particle and on its orientation relative to the plane of observation. Under such conditions it is advisable from our experience to divide the particle traces into two classes only; the first one contains the low velocity tracks and a second one the rest. The cut between the classes should be chosen so that the low velocity region contains only the big particles. Otherwise traces from rapid but large particles appear in the low velocity channel. It should be pointed out that even in this worst case extraction of the slow and bright traces is quite satisfactory.

At the discussion of the intensity dependence from the velocity it was implicitly assumed that the velocity will be constant for the period during which a tracer image passes by a pixel of the CCD. For high velocities this assumption will be approximated quite well, as the particle needs only a short time for the passage, whereas for low velocities the situation may become different. The change of direction of motion, for instance, will generally not take an infinite period of time. To get a feel on how the results depend on time-dependant motion, particle size and period of observation, we consider the simple case of a linearly oscillating sphere. Let the diameter of the sphere, its angular frequency of oscillation, and amplitude be D , Ω , and A , and the momentary values of the velocity and of the location of the centre of the sphere are v and x , respectively.

$$x/A = \sin(\Omega t) \quad (4)$$

$$v/(A\Omega) = \cos(\Omega t) \quad (5)$$

$$\Omega = 2\pi/T \quad (6)$$

Then, the time $t_1(x_1)$ that is needed to shift the centre of the sphere from:

$$x_1 - D/2 \text{ to } x_1 + D/2 \text{ for } x_1/A: -1 + D/A \leq x_1/A \leq 1 - D/A$$

will become:

$$t_1(x_1) = \Omega^{-1} (\arcsin(x_1/A + D/2A) - \arcsin(x_1/A - D/2A)) \quad (7)$$

As t_1 is directly proportional to the light energy collected on a pixel at point x_1 on the centre of the trace, the dimensionless velocity v_{int} calculated from an intensity measurement will become:

$$v_{\text{int}}(x_1, D/A) = D/(A\Omega x_1) \quad (8)$$

In a similar way, a corresponding expression for the velocity calculated from the intensity distribution in the regions of

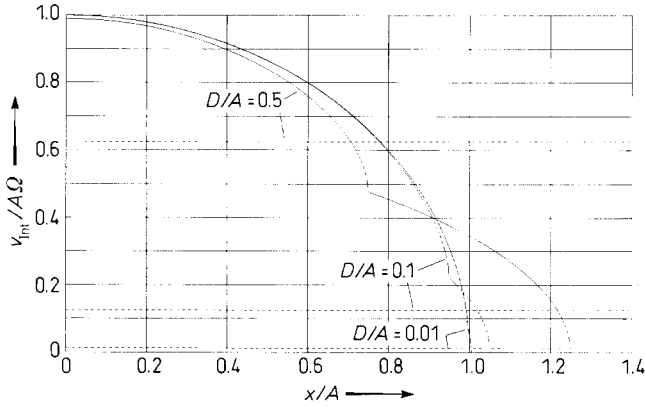


Fig. 3. Velocity v_{int} calculated from the brightness of the image of a linear oscillating sphere for different values of D/A . The velocity v (centre of the sphere) is displayed by a dotted line. The dashed lines indicate the corresponding minimum detectable velocities for an integration period of 40 ms. Velocities are normalized with the maximum velocity $A\Omega$ of the oscillation

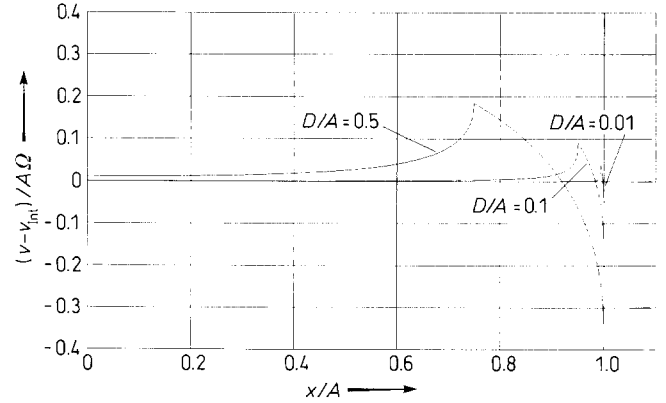


Fig. 4. Difference between v and v_{int} for different values of D/A . Velocities are normalized with $A\Omega$

direction reversal:

$$\pm 1 - D/(2A) < x_1/A < \pm 1 + D/(2A) \tag{9}$$

is easily found. These regions will be covered only by parts of the image of the oscillating sphere. As an example, v_{int} is displayed in Fig. 3 for D/A equal to 0.01, 0.1, and 0.5, respectively. The larger the diameter of the sphere the larger v_{int} at $x/A = 1$ (the point of direction reversal) will become and the more the location of $v_{int} = 0$ will be shifted to the outside. For $|x/A|$ up to $1 - D/A$ the deviation from the true velocity v (given by Eq. (5) and displayed by a dotted line) is approx. 5% for the spheres considered here. Outside this region, the velocity deviations increase strongly. The break in the curve is at a distance $x/A = 1 - D/(2A)$. The graph in Fig. 4 displays the difference between v and v_{int} directly. It shows how the velocity deviations depend on the ratios of D/A and on the actual value of x/A .

The value of $v_{p_{min}}/(A\Omega) = D/(A\Omega t_E)$ that gives the minimum detectable dimensionless velocity must also be taken into consideration. For $t_E = 40$ ms, $A = 1$ cm, and $\Omega = 20$ s⁻¹ and diameter ratios $D/A = 0.5, 0.1, 0.01$ the corresponding values of $v_{p_{min}}/(A\Omega)$ will become 62.5%, 12.5%, 1.25% of the maximum oscillation velocity (see Fig. 3). One possibility for increasing the resolution for a given particle size has already been mentioned. It simply consists in a prolongation of the integration time. The VFG-100 supports real time analysis, and a reduction of $v_{p_{min}}$ up to a factor of 24.5 is immediately possible. The velocity resolution for $D/A = 0.5$ may then become as low as 2.5%. Much more preferable, of course, would be a reduction of the tracer diameter, by which also the differences between the true and measured velocity will become smaller. From this arguments it is obvious that for optimum performance of the experimental set-up a proper choice of all physical parameters has to be made.

Finally, it should be mentioned that for velocity measurements the assumption of constant luminant flux across the

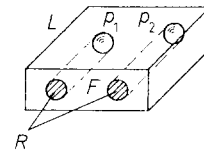


Fig. 5. Projection R of two tracer particles p_1 and p_2 on the plane of observation F . L is the depth of the probe volume

particle image is too coarse. For this purpose, as will be shown later one needs spherical tracers with homogeneous scattering properties.

2.5 Seeding of the flow

To get acceptable results, also the tracer concentration has to be matched properly. Let N_0 be the number density of the spherical particles and D their diameter. Then, in a duct of depth L (Fig. 5) the projection of the particles onto the plane of observation F that is perpendicular to L will cover an area R :

$$R = F \cdot L \cdot N_0 \cdot \pi \cdot D^2/4 \tag{9}$$

For $N_0 = 1000$ l/cm³, $L = 1$ cm, and $D = 0.01$ cm we will get: $R/F = 0.079$, i.e. approximately 8% of the cross section will be covered by particles. That means that the average light intensity on the corresponding site of the sensor of the CCD-camera will amount to 8% of the intensity of a particle image at rest. From the 64 grey levels mentioned above the lower five ones will be below the mean intensity and therefore will be confused with the background. A corresponding statement holds of the dark field mode of operation.

Additionally we need an estimation of how much of the field of view F will be covered by the traces during the integration period. To get an idea we assume as an example a plane parabolic velocity profile with:

$$u/u_0 = 1 - (2x/L)^2 \tag{10}$$

With: $N = N_0 \cdot F \cdot dx$ the number of particles within a strip of thickness dx and cross section F , the projection $P(u)$

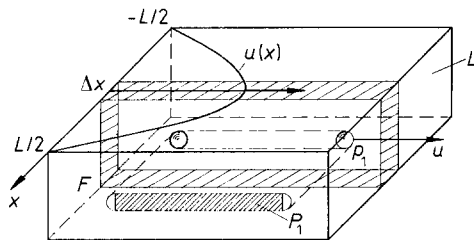


Fig. 6. Projection P_1 of the trace of particle p_1 on the plane of observation F for a time period t_E . The particle p_1 is moving at speed u . Starting- and end-point of the sphere are inside the probe volume. A plane parabolic velocity profile is assumed. L is the depth of the probe volume

(Fig. 6) of the traces during the integration time t_E on F for the velocity range $u_1 \leq u \leq u_0$ will become:

$$P(u_1) = N_0 \cdot F \cdot 2 \cdot \left[D \cdot t_E \cdot \int_{x_0}^{x_1} u(x) dx + \pi \cdot (D^2/4) \cdot \int_{x_0}^{x_1} dx \right] \quad (11)$$

$$= N_0 \cdot F \cdot 2 \left[D \cdot t_E \cdot u_0 \cdot (x_1 - 4 \cdot x_1^3 / (3 \cdot L^2)) + \pi \cdot D^2 \cdot x_1 / 4 \right] \quad (12)$$

with:

$$x_0 = 0, \quad \text{and} \quad x_1 = L/2 \cdot |(1 - u_1/u_0)^{1/2}|$$

The second term in Eqs. (11), (12) considers the contribution due to Eq. (9). It is in many practical cases a negligible quantity. From Eq. (12) it follows that, for the above mentioned set of parameters and a velocity u_0 of 16 cm/s, the particle traces will cover during 40 ms the field of view F by a factor of: $4.26 + 0.08$, and those in the velocity range $0 \leq u \leq 10.8$ cm/s already cover the entire field of view once. Below 10.8 cm/s which corresponds to the grey levels from 43 to 64 a resolution of the particles traces will not be possible in general for this choice of parameters. Here, for instance, a reduction of the tracer number density will help.

Much more stringent for a *simple* evaluation of the velocity also in the lower range are the restrictions due to the nonhomogeneous lateral brightness of a trace that arise from the shape, size, and scattering properties of the tracers, from the proportion of their images to the size of a pixel, and from the type of motion they perform. For the present task of extracting the low velocity streaks with their relatively large intensity changes these restrictions play practically no role as otherwise only short sections of a trace would be visualized at a time.

3 Experiments and results

The experimental setup used is displayed schematically in Fig. 7. It consists of a rotating duct, a CCD-camera for the capture of the images, and a PC with an image processor.

The torus shaped duct is cut into a Plexiglas disc and has a square cross section of 1×1 cm. Its front side is closed by a plane disc that is also made from Plexiglas. The mean radius of curvature of the duct is 15 cm. The torus can be

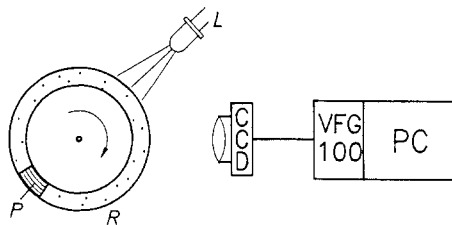


Fig. 7. Scheme of the experimental set-up. R : Rotating duct filled with a suspension of a glycerol-water-mixture and tracer particles, P : piston gliding inside the duct, L : light source, CCD : semiconductor camera for the capture of the tracer images. $VFG-100$: image processing board contained in a PC

rotated in a vertical plane around its main axis of symmetry at a prescribed number of revolutions. The flow is generated by a piston sliding inside the torus due to gravitational forces. The cross-section of the piston amounts to 80% to that of the duct. As a flow medium a mixture of glycerol and water (viscosity 6.2 cP) is used. For this velocity the duct can also be operated in a Re-number region where unsteady motion appears.

Three different kinds of tracers have been tested. Type 1 has a mean diameter of approx. $150 \mu\text{m}$ and is composed of coagulated spherical plastic particles of a yellowish colour. The size of a single element is about 10 to $30 \mu\text{m}$. The shape of these tracers is very compact and they scatter the light quite well due to the large and structured surface. With time, however, they disassemble into smaller agglomerates. The second type are DOW Uniform Latex particles of $90.6 \mu\text{m}$ with a standard deviation of $17.7 \mu\text{m}$. They are hardly visible in the fluid medium as their index of refraction does not differ very much from that of the flow medium. If they are illuminated from the side the light scattered from their surface is very inhomogeneous. The third type of tracers is made from pigments that are used for the preparation of iridescent colours. Their shape is like a flat disc of approx. $2 \mu\text{m}$ of height and a diameter of about 5 to $15 \mu\text{m}$. With their large mirror-like surfaces they are reflecting the light strongly but only into selected directions. As their orientation within the flow for most of the time is parallel to the plane of maximum shear they will generate bright tracers at a distinct angle of observation if illuminated with parallel light. From time to time, however, these particles execute a rotation and hereby the corresponding traces show large intensity fluctuations. For the experiments described here only tracers of type 1 will be shown.

The circular channel is illuminated by a tungsten low voltage lamp in radial direction and observed in the direction of its symmetry axis (dark field mode). An indirect illumination that would be much better is difficult to realize due to the unwanted light reflected from the duct walls.

In the bright field mode the nearly parallel light beam enters the probe volume at an angle of 0° relative to the axis of observation. As the particles available to us up to now are too transparent the dynamic is very poor. On the other hand

the bright field mode is very suitable for 3D visualization, Bartels (1991). We hope to dispose of suitable tracers in the near future.

A typical non-processed image of the tracer particle suspension of type 1 at rest is shown on the video-print in Fig. 8a. It looks like a cloud of more or less bright points bounded on both sides by the walls of the circular duct. The number density of the particles is about 100 l/cm^3 . The side walls of the circular duct become visible by the light scattered mainly from the corners of the duct. The other lines parallel to the walls are due to scattering from the key-beds that hold the washers to seal the front wall of the duct. Illumination is from the right side. The region marked in Fig. 8a by a cursor is displayed at an eighthfold expansion in Fig. 8b. The images of the particles are composed of more or less bright dots that are of square shape. At this expansion factor the pixel structure becomes visible. The offset and dynamic range of the 8-bit A/D converter of the processor is

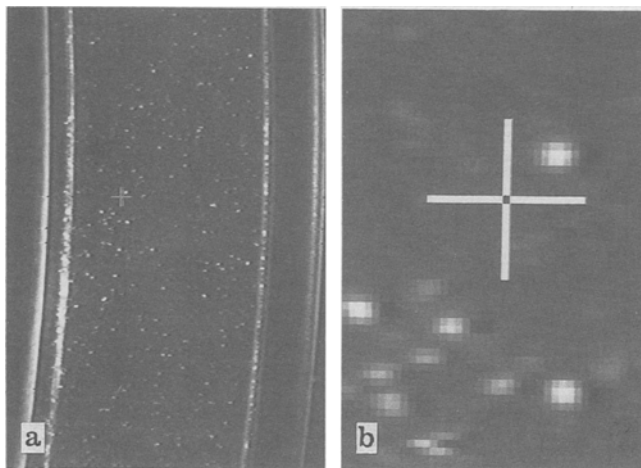


Fig. 8 a and b. Probe volume at rest state observed in the dark field mode. The duct is filled with a suspension of tracers of type 1 (a). Their size is displayed at an eighthfold expanded view (b). The pixel structure and the different grey levels of the tracer images become visible. Depth of field: 1 cm

adjusted such that it displays the information contained in the video signal by 256 grey levels.

To give a feel of the effect of digital filtering, the threshold for the grey levels is decreased stepwise from 255. The brightest pixel of the image in the right upper quadrant of the cursor appears at a grey level of 211 (Fig. 9a), and a second one shows up at 195 (Fig. 9b). Pixels with intensities larger than or equal to the threshold setting are preserved while the rest is set to zero. The result is displayed as a so-called binary image that contains only black or white pixels. The lower the threshold the more pixels appear. Partly they are due to new emerging but darker particle images and partly they are used to complete already existing images (Fig. 9 a–g). One realizes immediately that 1. not all particles images visible in Fig. 8 have passed the filter and 2. those that have passed will cover a smaller area as long as the peripheral intensity of the image is lower than the threshold setting. This example shows that in reality tracer images generally will be composed of pixels of different intensity.

When the duct starts rotating the tracer particles are conveyed with the flow medium and their images will be transformed into lines. The higher the velocity of a particle the longer and darker the streak will become if observation is in the dark field mode. Fig. 10a shows as an example an unprocessed full frame image as it is captured by the interline camera. The velocity of the piston relative to the duct is 22.6 cm/s . Each of the two fields is exposed for 40 ms but shifted against each other in time by 20 ms. So, a period of 60 ms is covered. For this exposure time, we expect that there are some not too short traces that start and end inside the probe volume which has an axial extension of 2.6 cm. To demonstrate this shift that may also be used to determine the flow direction, the image in Fig. 10a is passed through a digital filter with an upper level of 71 and a lower one of 58 (Fig. 10b). By this setting we reduce the background noise generated partly by the fast traces and suppress most of the bright traces that are due to slow and big tracers which generate very short and broad streaks. First, it is surprising how many traces that are hardly visible on the unfiltered original can be detected on Fig. 10b. A twofold expansion of

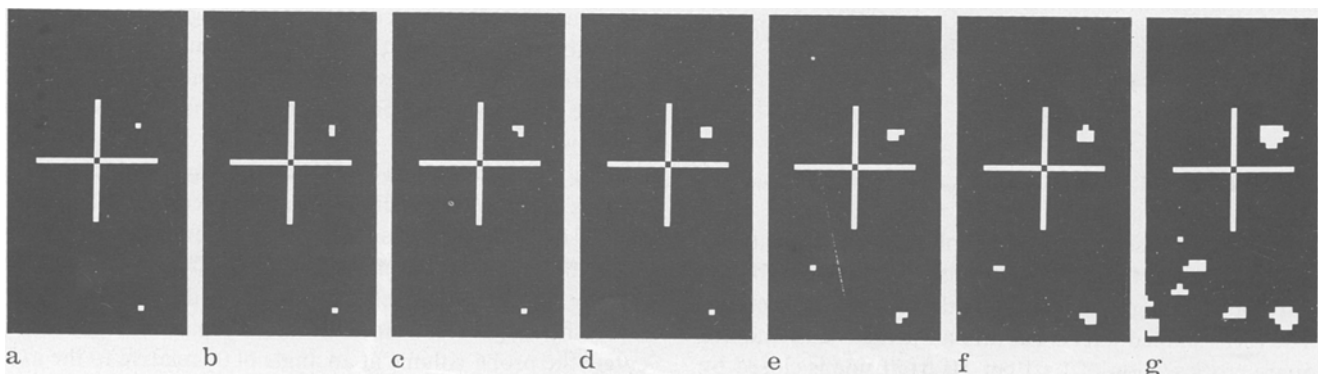


Fig. 9 a–g. Binary images of Fig. 8b at different threshold settings “ L ”; a $L = 211$; b = 195; c = 193; d = 188; e = 167; f = 138; g = 71. Pixels with grey levels $\geq L$ are preserved and displayed in (white) the rest is reset to black

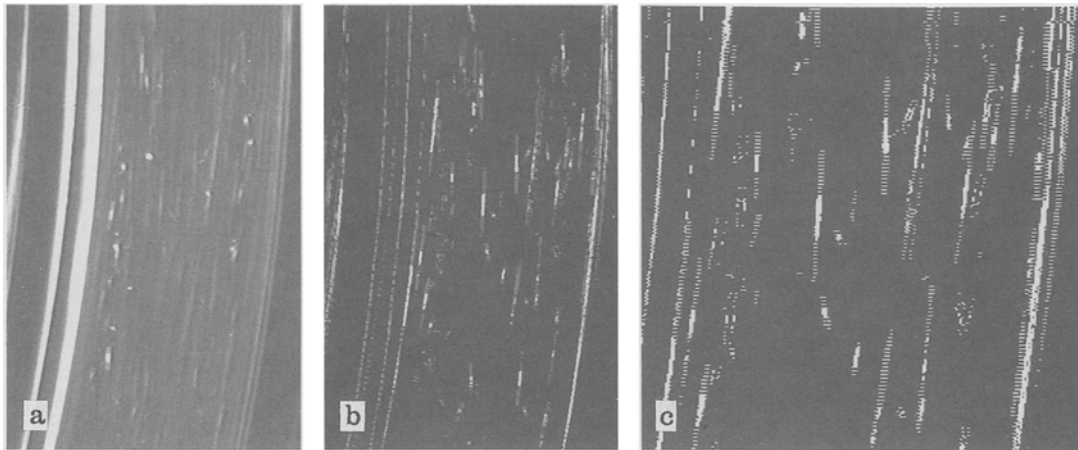


Fig. 10 a–c. Particle traces in the rotating duct at 14.4 r.p.m.; **a** unfiltered image, one full frame, tracer particles type 1; **b** high velocity traces accentuated by filtering; **c** two-fold expanded view, field structure of the image is visible

the region in Fig. 10c shows that the centre part for most of the tracers covers the even and odd field of the frame. As the image processors and sometimes even the videoprinters are able to display separately the odd or even video fields, one immediately knows which part of the trace has been captured first by the camera with respect to time.

Before presenting an example for the actual problem of visualization of low velocity paths some additional remarks for a better understanding of the flow system shall be made. Up to a certain Re-number the flow generated in the rotating duct is steady for an observer fixed with the gliding piston (Fig. 11 a). It corresponds – with certain restrictions – to the flow generated by a train running in a curved tunnel. As the piston is at rest with respect to the lab, simple results may be expected if the flow is observed from the lab. The net flux through a cross-section of the duct with respect to the lab is very low due to the small leakage through the gap between the piston and the wall. Therefore the velocity profile will be such that within the core region of the duct the axial flow direction will be opposite to the motion of the duct while in the outer region up to the walls of the duct the flow direction coincides with that of the wall (Fig. 11). As the axis of the duct is curved (radius of curvature is 15 cm) a secondary flow comes into existence that can be described by two counter-rotating vortex rolls with their axes aligned parallel to the axis of the duct. In the symmetry plane of the duct the secondary flow is directed from the inner radius to the outer one and in the neighbourhood of the side-walls their direction is reverse. A particle tracer that crosses due to secondary motion the interface $v_{ax} = 0$ will therefore change its direction with respect to the axis of the duct (Fig. 11 b). In the experiments the projections of the traces onto the front wall of the duct are observed. Two examples with the tracer suspension of type 1 that has also been used in Fig. 10 may be presented (Fig. 12). 24 successive frames are filtered digitally on-line and stored in the image processing board. The observation period covers 980 ms. The above-mentioned time-

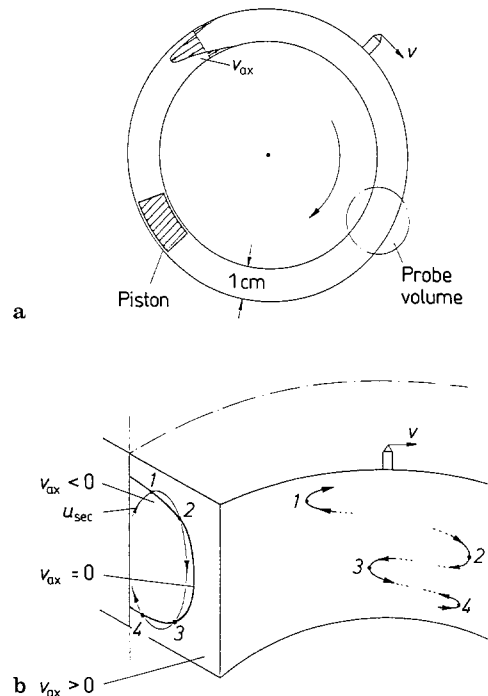


Fig. 11 a and b. Schematic display of the flow field. **a** vertical symmetry plane of the duct; **b** location of $v_{ax} = 0$ in an azimuthal cross section and scheme of a secondary streamline u_{sec} . Projection of particles on the plane of observation crossing the surface $v_{ax} = 0$ at points 1–4. Only the front part of the duct up to the symmetry plane marked by a dashed line is displayed

shift of the video-fields becomes effective only for the first and the last frame of a series. As it was to be expected the traces are clearly visible and they really cross the surface $v_{ax} = 0$.

In the vicinity of axial flow reversal the shape of the traces may be used to calculate the ratio of the projections of the axial to the radial velocity component onto the plane of observation. Under the plausible assumption that the gradi-

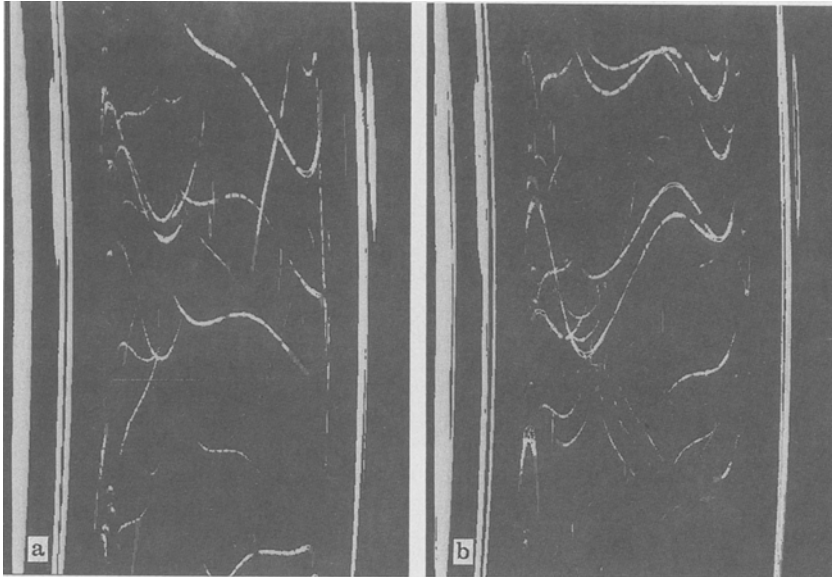


Fig. 12 a and b. Visualization of the low speed traces at two different Re-numbers; **a** $Re = 659$ (23 r.p.m.); **b** $Re = 815$ (28.5 r.p.m.). Duct rotates clockwise, depth of field ≈ 6 mm, scale 1:0.38

ent of v_{ax} and the azimuthal (secondary) velocity components are constant in a small region, parabolic shaped particle traces are expected. Generally one or two directional reversals of a trace will be observed for the present choice of the parameters, and only from time three successive reversals appear.

Adjacent to the inner and outer side-wall of the duct there is a ring-shaped section where no “slow” traces are to be seen. There, the axial component of the flow velocity along the entire depth of the channel decreases continuously from wall velocity to $v_{ax} = 0$. The position of the inner and outer radius of the projection of the torus shaped surface $v_{ax} = 0$ is defined by the flow reversals closest to the corresponding side-walls. No indications have been found from the images that the surface $v_{ax} = 0$ coincides over a larger distance with a streamline.

A closer look to the particle traces in the neighbourhood of flow reversals show that their width decreases at increasing distance from the apex. This effect is due to the increasing velocity of the tracer. It is the only information on the velocity still available on a digitally filtered image. The large interruptions of the traces visible in Fig. 12 are due to the shading effect of the bolts that fix the front wall of the duct, the small ones are a consequence of the filter that cuts away the ends of the traces that are of lower intensity. They may be used as time marks.

The traces observed up to now were only a few pixels in width. For such cases the aforementioned fluctuations of the intensity cannot be excluded. Evaluation of the velocity will therefore result into more or less qualitative values sufficient for a coarse classification as has been shown above. In the following, we will try to find out the chances to develop this observation technique into a quantitative method. First of all, we need traces larger in width to get a better spatial resolution. From the possibilities discussed above we in-

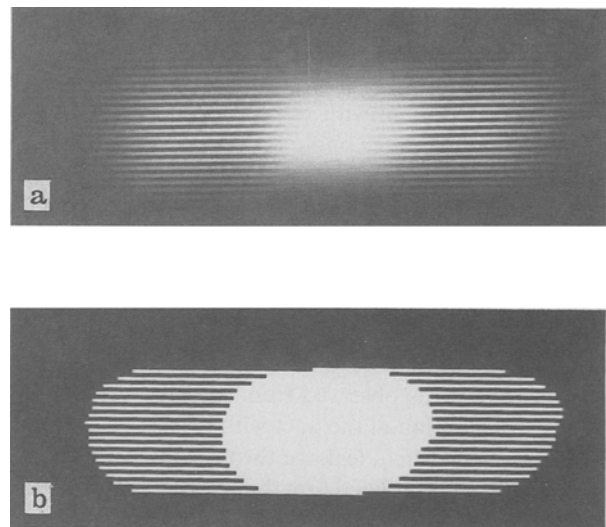


Fig. 13 a and b. Particle trace captured at a scale of 1:2.4; **b** contours of the trace enhance by binary filtering. Exposure time: 60 ms (one full frame)

crease the scale of observation and keep to the particles of type 1. Figure 13a shows an unprocessed image of a moving particle taken at a scale of approx. 1:2.4. The width of this trace is about 35 pixels. For the camera used the field of view is reduced now to about 3.7×2.8 mm². Some ten to 30 traces are easily placed within this format. In Fig. 13b the contours of the trace are enhanced to improve the visibility. By this procedure the even and odd fields that form a frame are clearly visible. In Fig. 14 the contours of the isointensity lines of this trace are displayed in steps of 20 grey levels. The width of a line amounts likewise to 20 grey levels. If the particle image stays within the field of view during the period of observation the isointensity lines form closed loops. For

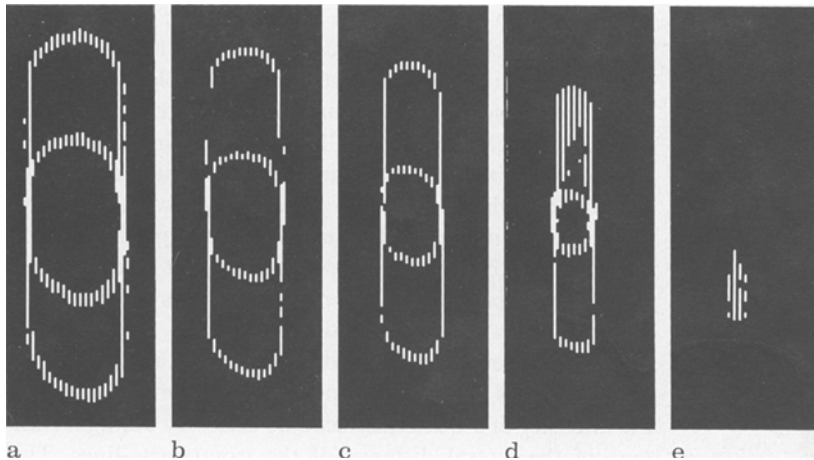


Fig. 14 a–e. Isointensity contours of the trace from Fig. 13 in steps of 20 grey levels. Width of the lines 20 grey levels. **a** 40–60; **b** 80–100; **c** 120–140; **d** 160–180; **e** 200–220

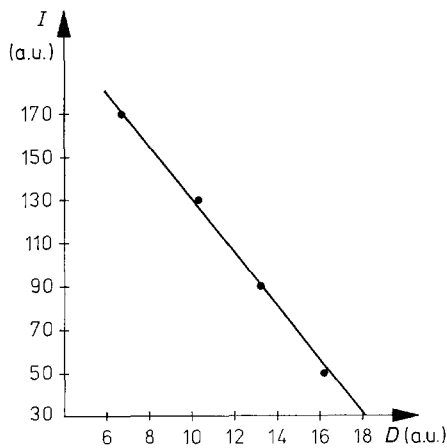


Fig. 15. Dependence of the intensity I from the lateral distance D of the isointensity lines evaluated from Fig. 14

the case that the centre of the image trajectory is a straight line, the isointensity curves are symmetrically arranged to both sides of the path. For constant velocity they are additionally parallel with exception of a small region (about one velocity radius) close to both ends of the trace. For longer traces, generally only the straight side parts of the loops will be observed. In the example of Fig. 14 eight different grey level zones can be immediately extracted without any further interpolation. The velocity of the particle image is evaluated from the shift of the position of the image in the two fields, that are separated in time by 20 ms.

The information contained in the isointensity lines of Fig. 14 can immediately be used for gauging the dependence of the intensity of a trace from the velocity of the particle image. For this purpose, the lateral distance D between the straight sides of each isointensity line is measured and displayed versus the intensity I either in a graph (Fig. 15) or approximated by an interpolating function. The application of the graph is very simple if one recalls that an increase in particle velocity by a factor of α will result – for a fixed value

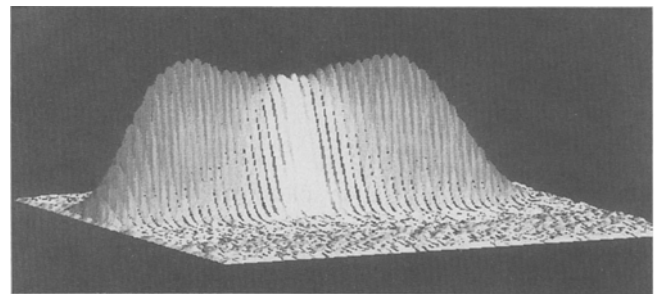


Fig. 16. Perspective view of the 3-D intensity distribution of a particle trace in expanded view. Exposure time: 60 ms

of D – into a reduction of the intensity I by the same factor. In order to evaluate the velocity from the intensity of a trace generated by a particle of unknown velocity but otherwise equal properties and for the same configuration of the set-up, one simply has to measure the lateral distance D_{new} of a suitable isointensity line I_{new} . Then, one evaluates from the graph $I(D_{\text{new}})$. The velocity of the particle will then be $[I(D_{\text{new}})/I_{\text{new}}(D_{\text{new}})] \cdot v_0$, with v_0 the gauging velocity. The use of the lateral intensity distribution has the advantage that one particle type may serve both, for the measurement for low velocities (outer regions of the spheres) and for the higher velocities (inner regions) as many CCD devices are quite insensitive against overexposure and blooming.

As can be seen from Fig. 14 d–e the intensity distribution along the trace increases a little bit and that one in Fig. 16 that has been evaluated for another particle shows two bumps. This is probably due more to the unsymmetric shape of the tracer (type 1) than to a velocity change. The deviations from an ideal shape become visible as the particles are moving in a strong shear field and therefore execute rotations. To improve velocity resolution, particles that are more homogeneous in size and scattering properties have to be applied.

From the shape of the isointensity lines in Fig. 14 one can see that the maximum intensity is reached earlier than ex-

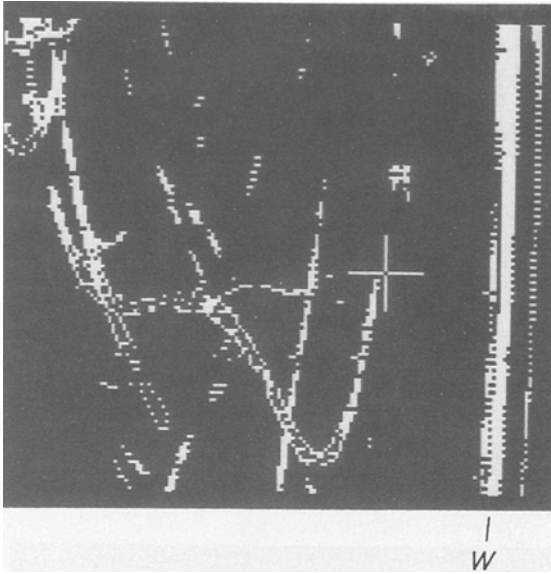


Fig. 17. Isointensities of traces taken at a scale of 1:0.22 and displayed in fourfold expanded view, *W* right side-wall of the duct

pected from the simple model of constant flux across the particle image. This effect reduces the minimum detectable velocity as the particle appears to be smaller and is responsible for the nearly linear decrease of the lateral intensity distribution of a trace.

By proper selection of the iso-intensity level a coarse visual inspection of the velocity becomes possible also from particle traces only a few times larger than a pixel (i.e. for a larger field of view than that of Fig. 14). The trace marked by the cursor (Fig. 17) shows how the corresponding particle shows up at a comparatively high velocity, decelerates, changes three times its direction of motion, before it becomes faster again and disappears. Even though the iso-intensity in Fig. 17 is very often interrupted and is similar more to a dashed line than to a continuous curve, the trace is quite well discernible and not too much disturbed by the crossings with other traces. Since binary filtering is performed after capture of the image one has sufficient time to select a suitable velocity range.

4 Conclusions

Despite the simplicity of this technique it is surprising how much qualitative but also quantitative information can be

extracted from a single frame, a fact which is mainly due to the progress achieved in image processing within the last few years. Of course, there are still many problems. Some of them are of more technical nature and there already exist appropriate solutions, like CCD-cameras with a higher resolution, both, in physical as in dynamic range, and image processors with a larger storage capacity. Also more appropriate scattering particles, e.g., by adding (fluorescent) colours to the base material are available, but there seems to be a need for production of new tracers and systematic testing of particles available on the market.

On the other hand automatic recognition and processing of the traces is still at its infancy. The problem of analyzing the intensity of a track may become easier by taking advantage of the lateral distance of the iso-intensity-lines. This method could also be helpful for the observation of the rotary motion of flat tracers in shear fields, that will result into a strong intensity modulation of the trace.

For velocity measurements, of course, only spherical particles that are also good scatterers will be acceptable. If their size is not sufficiently homogeneous one will at least be able to measure the velocity ratio along one trace.

Further efforts are necessary, especially if 3-D evaluation of a flow field is to be included. Here, the intensity of a trace may be helpful for the reconstruction of the images. In contrast to single point temporal measuring techniques like LDV or hot wire anemometry which surely will be of higher accuracy, the present technique offers the possibility of performing simultaneous temporal and spatial measurements.

References

- Adrian, R. J. 1988: Optical methods for measuring vector fields. I – Principles; II – Techniques, Brussels: von Karman Institute for Fluid Dynamics Lecture Series.
- Bartels-Lehnhoff, H.-H. 1991: Erfassung dreidimensionaler Bahnlinien und Geschwindigkeitsfelder mittels automatischer Bildverarbeitung. Mitt., Max-Planck-Inst. Strömungsforsch. 101
- Brodkey, R. S. 1986: Image processing and analysis for turbulence research. Chem. Eng. Educ. 20, 202–207
- Jähne, B. 1989: Digitale Bildverarbeitung. Berlin, Heidelberg, New York: Springer
- Merzkirch, W. 1974: Flow visualization. New York: Academic Press
- Reynolds, O. 1883: Phil. Trans. 174, 935–982; Scientific Papers 2, 51
- Wuest, W. 1969: Strömungsmeßtechnik. Braunschweig: Vieweg

Received November 13, 1991